
Differentiable Sparsification for Deep Neural Networks

Yongjin Lee

Electronics and Telecommunications Research Institute
281 Gajeong-ro, Yuseong-gu, Daejeon, Korea 34129
solarone@etri.re.kr

Abstract

Deep neural networks have relieved a great deal of burden on human experts in relation to feature engineering. However, comparable efforts are instead required to determine effective architectures. In addition, as the sizes of networks have grown overly large, a considerable amount of resources is also invested in reducing the sizes. The sparsification of an over-complete model addresses these problems as it removes redundant components and connections. In this study, we propose a fully differentiable sparsification method for deep neural networks which allows parameters to be zero during training via stochastic gradient descent. Thus, the proposed method can learn the sparsified structure and weights of a network in an end-to-end manner. The method is directly applicable to various modern deep neural networks and imposes minimum modification to existing models. To the best of our knowledge, this is the first fully [sub-]differentiable sparsification method that zeroes out parameters. It provides a foundation for future structure learning and model compression methods.

1 Introduction

The success of deep neural networks (DNNs) has changed the paradigm of machine learning and pattern recognition from feature engineering to architecture engineering [16, 14, 22, 7, 32]. Although DNNs have relieved the burden of feature engineering, comparable human efforts are instead required to design an effective architecture, such as by determining the number of neurons or layers and the connections between nodes. In addition, as DNNs grow ever larger (even up to 10–68 million parameters) [8, 10, 15, 32], a considerable amount of effort is also being invested in reducing the sizes of existing models and in being able to deploy such networks on constrained platforms with acceptable latency periods [26, 25].

These problems can be addressed by sparsification of an over-complete model [20]. A network structure can be carved out of an over-complete model by removing redundant blocks [3, 29] or deleting unnecessary connections between nodes or blocks [2, 18, 30], which also reduces the network size. Among several approaches, pruning has long been adopted [17, 6, 26, 19, 5]. It typically applies several steps to a pre-trained model (select the unimportant parameters of a pre-trained model, delete those parameters, and retrain the pruned model) and may repeat each of these steps multiple times. Another popular approach is sparse regularization with a proximal gradient [21, 3, 29, 33], which shrinks redundant parameters to zero during training and does not require a pre-trained model. Among the most popular tools is l_1 -regularizer [28]. However, as it acts on an individual parameter, it often produces unstructured irregular models; thus, its use diminishes the benefit of parallel hardware computation, such as that done through GPUs [29]. In order to obtain regular sparse structures, a sparse regularizer with $l_{2,1}$ -norm [3, 29] was adopted on a group of parameters so that all parameters under the same group are either retained or zeroed-out together. By zeroing-out parameters at the group level, it is possible to determine the number of neurons or layers automatically as a part of

the training process. However, the regularization terms are optimized in a separate process from the gradient descent-based optimization process for prediction loss. The update rules should be implemented manually and the approach is limited to cases in which closed-form solutions for the proximal operation are known.

In this work, we propose a fully [sub-]differentiable sparsification method for DNNs, which directly optimizes a regularized objective function and allows parameters to be exactly zero during training via stochastic gradient descent. Thus, the method can simultaneously learn the sparsified structure and weights of DNNs in an end-to-end manner. It does not require manual coding of a pruning step or an update rule like a soft-thresholding operator, and it allows for simpler implementation. It can adopt various norms as a regularizer regardless of whether or not the closed form solutions for the proximal operator are known. Another advantage of the proposed method is that it can easily be applied to a group of parameters or a building block; thus, it can produce a structured model and maximize the benefits of parallel hardware computation (e.g., GPUs) and it suits the trend towards modularized design in deep learning [22, 27, 7, 32].

2 Related Work

2.1 Proximal Gradient

Our proposed method is related to sparsity regularization with a proximal gradient [21]. A regularized objective function is written as

$$\mathcal{L}(D, W) + \lambda \mathcal{R}(W), \quad (1)$$

where \mathcal{L} denotes a prediction loss, \mathcal{R} is a regularization term, D is a set of training data, W is a set of model parameters, and λ controls the trade-off between prediction loss and model complexity. The most popular regularizer is l_1 -norm,

$$\mathcal{R}(W) = \sum_i |w_i|, \quad (2)$$

where w_i is an individual element of W . To optimize the regularization term, parameter updating is performed with a proximal operator,

$$w_i \leftarrow \text{sign}(w_i) (|w_i| - \eta\lambda)_+, \quad (3)$$

where \leftarrow denotes an assignment operator, η is a learning rate, and $(\cdot)_+$ represents $\max(\cdot, 0)$. As this approach acts on an individual parameter, it often produces unstructured irregular models. In order to obtain regular sparse structures, the sparse regularization with $l_{2,1}$ -norm can be adopted [3, 29]. All parameters in the same group are either retained or zeroed-out together. Regularization with $l_{2,1}$ -norm can be written as

$$\mathcal{R}(W) = \sum_g \|\mathbf{w}_g\|_2 = \sum_g \sqrt{\sum_i w_{g,i}^2}, \quad (4)$$

where $W = \{\mathbf{w}_g\}$ and \mathbf{w}_g represents a group of model parameters. The regularization term is optimized with a proximal operator,

$$w_{g,i} \leftarrow \left(\frac{\|\mathbf{w}_g\|_2 - \eta\lambda}{\|\mathbf{w}_g\|_2} \right)_+ w_{g,i}. \quad (5)$$

When a group has only one single parameter, it degenerates to l_1 -norm regularization.

Another related group regularization method is exclusive lasso with $l_{1,2}$ -norm [34, 33]. Rather than either retaining or removing an entire group altogether, it promotes competition or sparsity within the group. The regularization term is written as

$$\mathcal{R}(W) = \frac{1}{2} \sum_g \|\mathbf{w}_g\|_1^2 = \frac{1}{2} \sum_g \left(\sum_i |w_{g,i}| \right)^2, \quad (6)$$

and its updating rule is derived as

$$w_{g,i} \leftarrow \text{sign}(w_{g,i}) (|w_{g,i}| - \eta\lambda \|\mathbf{w}_g\|_1)_+. \quad (7)$$

These proximal operators consist of weight decaying and thresholding steps, and they are performed at every mini-batch or epoch in a separate step after the prediction loss is optimized. Therefore, some extra effort is required to implement the update rules manually. Moreover, the applications of this approach are limited to cases in which closed-form solutions for the proximal operator are known. In contrast, our approach directly optimizes a regularized objective function and allows parameters to be zero during training via stochastic gradient descent. It leads to simpler implementation and can employ various norms regardless of whether or not closed-form solutions for proximal operators are known, for example, p -norm with $p < 1$.

2.2 Differentiable Approach

Similar to our work, previous differentiable approaches [2, 18] learn the structure of a neural network by optimizing architecture parameters in a relaxed continuous domain, where architecture parameters represent the importance scores of building blocks or the connection strengths between those blocks. However, as the architecture parameters cannot be zero during training, the top k connections or components are stochastically or deterministically selected according to the values of the architecture parameters to derive a discretized architecture. Therefore, the approach may suffer from the discrepancy between a learned architecture and a final discretized one. Moreover, the value of k must be pre-specified manually; thus, the same value is set for all blocks or modules, which may be sub-optimal. In contrast, our approach drives the architecture parameters to zero by directly optimizing a regularized objective function. Doing so can minimize the model discrepancy, and a network can choose different numbers of components or connections for each module during the training process.

3 Proposed Approach

3.1 Base Model

We assume that there are n components in a module. A component can be any building block for a DNN or its output. For example, it can be a channel or a layer of a convolutional neural network (CNN) such as ResNet [7, 8] or DenseNet layer [10]. It can also represent a node in a neural graph [30] or a graph CNN [11]. A module represents a composite of components, such as a group of channels or a layer. For illustration purposes, we assume that a module \mathbf{y} can be written as the linear combination of components \mathbf{f}_i or the concatenation:

$$\mathbf{y}(\mathbf{x}) = \sum_{i=1}^n a_i \mathbf{f}_i(\mathbf{x}; \mathbf{w}_i) \text{ or } [a_1 \mathbf{f}_1(\mathbf{x}; \mathbf{w}_1), \dots, a_n \mathbf{f}_n(\mathbf{x}; \mathbf{w}_n)], \quad (8)$$

where \mathbf{x} denotes a module input, \mathbf{w}_i represents the model parameters for component \mathbf{f}_i , and a_i is an architecture parameter. The model parameters \mathbf{w}_i denote ordinary parameters, such as a filter in a convolutional layer or weight in a fully connected layer. The value of a_i represents the importance of component i or the strength of the connection between nodes in another context. Forcefully setting a_i to zero amounts to removing component \mathbf{f}_i or zeroing-out \mathbf{w}_i . Thus, creating competition between the elements of a and making them to be zero eliminates unnecessary components or connections. We will show that this simple sample model can be applied to various cases.

3.2 Differentiable Sparse Parameterization

First, we demonstrate how to parameterize architecture parameters with non-negative constraints, which is useful for an attention mechanism with the softmax function. To set up competition between the elements of a and allow them to be zero, we parameterize the architecture parameters as follows:

$$\gamma_i = \exp(\alpha_i) \quad (9)$$

$$\tilde{\gamma}_i = (\gamma_i - \sigma(\beta) \cdot \|\gamma\|_1)_+ \quad (10)$$

$$a_i = \frac{\tilde{\gamma}_i}{\sum_{j=1}^n \tilde{\gamma}_j}, \quad (11)$$

where α_i and β are unconstrained free parameters, $\sigma(\cdot)$ denotes a sigmoid function, and $(\cdot)_+$ represents $\text{relu}(\cdot) = \max(\cdot, 0)$. When a parameter is non-negative, the proximal operator of Eq. (7) is reduced to Eq. (10). Although the forms are similar, they have completely different meanings. The proximal operator is a learning rule, whereas Eq. (10) is the parameterized form of the architecture parameters, and is part of the neural network.

We can easily verify that a_i is allowed to be zero and is differentiable from a modern deep learning perspective. The free parameters α_i and β are real-valued and do not restrict a training process that uses a stochastic gradient descent algorithm. Thus, we can train a_i through α_i and β . The exponential function in Eq. (9) ensures that the architecture parameters are non-negative. Typically, a_i cannot be zero due to the exponential function in Eq. (9). However, $\tilde{\gamma}_i$ in Eq. (10) can be zero by the thresholding operation; hence, a_i can be zero as well. The term $\sigma(\beta) \cdot \|\gamma\|_1$ plays the role of a threshold. The thresholding operation is interpreted as follows: if the strength of component i in a competition group is low compared to the overall strength, it is dropped from the competition. Note that the scalar parameter β in Eq. (10), which determines the magnitude of the threshold, is not a hyper-parameter, but its value is automatically determined through training. Mathematically, the thresholding operator is not differentiable, but this should not be an issue considering the support of relu as a built-in differentiable function in modern deep learning tools. Additionally, γ is non-negative; thus, its l_1 -norm is simply the sum of γ_i (i.e., $\|\gamma\|_1 = \sum \gamma_i$). The softmax of Eq. (11) is also differentiable. The softmax is optional but useful when it is necessary to promote competition between components, as in the attention mechanism.

Similarly, a signed architecture parameter can be formed as

$$a_i = \text{sign}(\alpha_i) \left(|\alpha_i| - \sigma(\beta) \|\alpha\|_1 \right)_+, \quad (12)$$

where α and β are free parameters. The gradient of the sign function is zero almost everywhere, but this is not a problem for modern deep learning tools. The equation can be rewritten as

$$a_i = \begin{cases} (\alpha_i + \sigma(\beta) \|\alpha\|_1)_- & \text{if } \alpha_i < 0 \\ (\alpha_i - \sigma(\beta) \|\alpha\|_1)_+ & \text{otherwise,} \end{cases}$$

where $(\cdot)_- = \min(\cdot, 0)$. The gradient can be computed separately according to whether or not its value is negative. To the best of our understanding, TensorFlow [1] already deals with the sign function in the explained manner, so `tf.math.sign()` can be used without manually implementing the conditional statement.

3.3 Sparsity Regularizer

In the proposed approach, a regularized objective function is written as

$$\mathcal{L}(D, W, a) + \lambda \mathcal{R}(a), \quad (13)$$

where a denotes the vector of architecture parameters. Sparsifying a is equivalent to sparsifying a DNN. Therefore, the regularization term can be used on a to encourage the sparsity of the DNN. The proposed method is not limited to a particular norm. Also, different sparsity patterns can be derived depending on the type of norms. For example, the most popular choice for parameter selection is l_1 -norm, but it is unsuitable for a in Eq. (11) as it is normalized using the softmax function. The l_1 -norm of that parameter is always 1, i.e., $\|a\|_1 = \sum_{i=1}^n |a_i| = 1$. Therefore, we should employ p -norm with $p < 1$:

$$\mathcal{R}(a) = \left(\sum_{i=1}^n |a_i|^p \right)^{\frac{1}{p}} = \left(\sum_{i=1}^n a_i^p \right)^{\frac{1}{p}}, \quad (14)$$

where the second equality holds as a_i is always non-negative. To the best of our knowledge, a closed-form solution for the proximal operator of p -norm with $p < 1$ is not known and the proximal gradient method will not work. However, the regularization term is differentiable almost everywhere as is relu . Thus, the proposed approach can directly optimize the regularized objective function and zero-out components with stochastic gradient descent.

By simply switching one norm to another for the regularizer, it is possible to derive different sparsity patterns for a DNN. For example, an individual component can be removed with l_1 -norm (Eq. 2) and

a group of components or an entire module can be zeroed-out with $l_{2,1}$ -norm (Eq. 4). Note that it is not necessary to manually implement different updating rules as in the proximal gradient approach. Instead, we can simply rewrite a regularization term in the objective function. Examples codes and experimental results are shown in the supplementary material.

3.4 Rectified Gradient Flow

If γ_i in Eq. (10) or α_i in Eq. (12) is less than the threshold, the gradient will be zero, and the component will not receive learning signals. However, this does not necessarily mean that a component permanently dies once its importance score falls below the threshold. The component may recover because the threshold is adjustable and the importance scores of other components may decrease. Nevertheless, to ensure that the architecture parameters of dropped components continuously receive learning signals, we propose approximating the gradient of the thresholding function. As in [31], where the gradient of a step function was approximated using that of *leaky relu* or *soft plus*, we suggest employing *elu* [4] as a variant of the proposed method: *relu* is used in a forward pass, but *elu* is used in a backward pass.

This heuristic approach leads to a similar learning mechanism as that proposed in [30], where the gradient flows to dropped (or zeroed out) edges but does not flow through these dropped edges. The architecture parameters in our proposed method correspond to the edges in [30]. Note that our approach is easy to implement and does not require additional codes to select dropped edges and control the gradient flow. We simply optimize the objective function using approximated gradients. The implementation codes are shown in the appendix.

4 Application and Experiment

In this section, we show that the proposed approach can be used to reduce the size of a network as well as to learn the structure. Our aim is not to achieve state-of-the-art performance but to validate the basic idea and broad applicability of the proposed approach. In order to demonstrate its broad applicability using limited computing resources, we perform experiments with relatively small datasets, such as CIFAR-10/100 [13]. Our implementations closely follow those of baseline models, including in terms of the model structures and hyper-parameter settings.

4.1 Channel Pruning in a Convolutional Network

Table 1: Performance on CIFAR-10, DenseNet-100-BC-K12.

Model	Sparsity(%)		Top-1 Error(%)		Params		FLOPs	
	Avg.	Std.	Avg.	Std.	Avg.	Std.	Avg.	Std.
Base	00.0	0.0	5.44	0.11	7.6×10^5	0.0	5.8×10^8	0.0
NS	70.0	0.0	6.53	0.19	2.9×10^5	9.3×10^2	1.9×10^8	5.0×10^6
NS	80.0	0.0	8.39	0.28	2.0×10^5	2.0×10^3	1.4×10^8	3.4×10^6
DS	70.3	0.1	5.77	0.09	2.7×10^5	2.3×10^3	1.8×10^8	1.6×10^6
DS	80.4	0.1	6.64	0.11	1.7×10^5	0.6×10^3	1.3×10^8	2.0×10^6

Network-slimming(NS) [20] prunes unimportant channels in convolutional layers by leveraging the scaling factors in batch normalization. Let x_i and y_i be the input and output, respectively, of batch normalization for channel i . Then, the operation can be written as

$$\tilde{x}_i = \frac{x_i - \mu_i}{\sqrt{\sigma_i^2 + \epsilon}}; y_i = a_i \tilde{x}_i + b_i,$$

where μ_i and σ_i denotes the mean and standard deviation of input activations, respectively, a_i and b_i are scale and shift parameters, and ϵ is a small constant for numerical stability. The scaling parameter a can be regarded as an importance score or an architecture parameter, and the affine transformation can be re-written as

$$y_i = a_i (\tilde{x}_i + b_i).$$

By forcing a_i to be zero, the corresponding channel can be removed. Network-slimming trains an initial network with l_1 -regularization on a to identify insignificant channels. After the training, channels with small values of a are pruned. To compensate for the damage caused by pruning, a pruned network is re-trained. In our approach, we parameterize the scaling parameter using Eq. (12) and train a network with l_1 -norm on a using the stochastic gradient descent method without pruning and fine-tuning.

We perform comparative experiments on CIFAR-10/100 [13]. The training and test sets contain 50,000 and 10,000 samples respectively, and the final test error is reported at the end of training or fine-tuning on all training images. We adopt a standard data augmentation scheme (random shifting and flipping) as in [7, 8]. In the network-slimming method, λ in Eq.(13) is fixed at 10^{-5} , but in our approach, we vary its value to induce different levels of sparsity. DenseNet-BC-K12 (100 layers) [10] and ResNet (164 layers) [7, 8] are employed as base networks. In the network-slimming method, pre-trained models are obtained by training networks for 160 epochs with an initial learning rate of 0.1. The learning rate is divided by 10 at 50% and 75% of the total number of training epochs. After the training process is complete, channels with small values of a are removed and a slimmed network is re-trained for additional 160 epochs with the same settings as in the initial training, but the learned weights are not re-initialized. In our approach, we train networks for 320 epochs without fine-tuning or re-training. Network-slimming initializes the scaling factor at 0.5 and we set $\alpha_i = 0.5(n+1)/n$ and $\beta = \log(n^2 + n - 1)$ in Eq.(12) so that a_i starts at 0.5.

Table 1 shows the experimental results on CIFAR-10 with DenseNet. The results of more experiments, including those using ResNet and CIFAR-100, are shown in the supplementary materials. The authors strongly urge readers to peruse the supplementary materials. We ran each experiment 5 times; the data in the table are the average and standard deviation from these 5 repetitions. Our proposed method is called by *Differentiable Sparsification* (DS). We controlled the value of λ such that it has a similar sparsity rate as the network-slimming approach. In the tables, *sparsity* denotes the pruning rate, i.e, the number of removed channels in hidden layers. The experiments show that the proposed differentiable approach more effectively learns slimmed models than the other approach.

4.2 Discovering Neural Wiring

Table 2: Performance on CIFAR-10, Discovering Neural Wiring.

Model	Top-1 Error(%)		Parmas		Mult-Adds	
	Avg.	Std.	Avg.	Std.	Avg.	Std.
MobileNetV1($\times 0.25$)	13.44	0.24	2.2×10^5	0.0	3.3×10^6	0.0
No Update($\times 0.225$)	13.86	0.27	2.2×10^5	3.7×10^1	4.5×10^6	3.7×10^4
DNW($\times 0.225$)	10.30	0.20	1.8×10^5	6.7×10^1	3.1×10^6	4.6×10^4
PG- l_1 -norm	12.17	0.44	2.1×10^4	9.4×10^2	3.3×10^6	1.7×10^5
PG- $l_{1,2}$ -norm	13.62	0.56	9.6×10^4	1.6×10^4	3.4×10^6	8.6×10^4
DS-No Rectified Grad.	10.55	0.23	6.1×10^4	5.7×10^2	3.4×10^6	4.5×10^4
DS-Rectified Grad.	9.36	0.27	4.7×10^4	8.4×10^2	3.3×10^6	6.7×10^4

Discovering Neural Wiring(DNW) [30] relaxes the notion of layers and treats channels as nodes in a neural graph. By allowing channels to learn inter-channel connections, it simultaneously discovers the structure and learns the parameters of a neural network. An input to node v , \mathbf{y}_v , is expressed as

$$\mathbf{y}_v = \sum_{(u,v) \in \mathcal{E}} w_{u,v} \mathbf{x}_u,$$

where \mathbf{x}_u denotes the state of a preceding node, \mathcal{E} represents an edge set and $w_{u,v}$ is the connection weight of an edge. The structure of a neural graph can be determined by choosing a subset of edges. At each iteration of the training process, DNW chooses the top k edges with the highest magnitude, which is called the real edge set, and refers to the remaining edges as the hallucinated edge set. On the forward pass or at inference time, only real edges are used. As DNW allows the magnitude of the weights in both sets to change throughout the training process, a hallucinated edge may replace a real edge when it becomes strong enough. The weights of real edges are updated in an ordinary manner

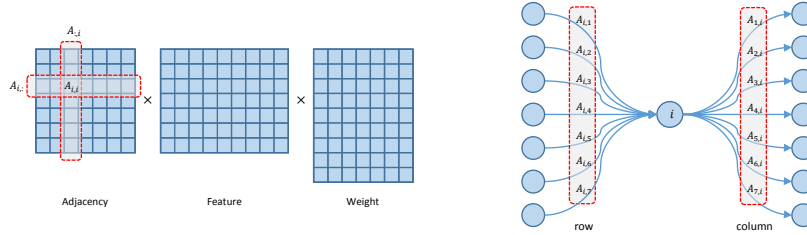


Figure 1: *Left*: Structure of a GCN block. Each block consists of a shared adjacency, an input feature, and a weight matrix. Each row and column of an adjacent matrix are treated as groups to enable learning of the relationships between a node (indexed by i) and its neighbors. *Right*: Row grouping creates competition between in-coming nodes, and column grouping creates competition between out-going nodes.

with stochastic gradient descent, but those of hallucinated edges are updated by a specialized leaning rule: the gradient flows to hallucinated edges but does not flow through them.

The architecture parameters in our proposed method correspond to the edges in DNW. We parameterize the edges using Eq. (12) and train a network with l_1 -norm on edges to induce sparsity. The rectified gradient leads to an update rule which is similar to that of DNW: the rectified gradient ensures that dropped architecture parameters continuously receive learning signals by approximating the gradient of the thresholding function. However, it is not necessary to keep track of the real and hallucinated edge sets. We simply optimize the objective function with approximated gradients. The rectified gradient can be implemented in a couple of lines using modern deep learning tools; the relevant code is shown in the supplementary material.

We perform experiments on CIFAR-10/100 [13]. The final test error is reported at the end of the training process. MobileNetV1 ($\times 0.25$) [9] is employed as a base model and our implementation closely follows that of DNW. We train the model for 160 epochs with an initial learning rate of 0.1. The learning rate is scheduled using cosine annealing. For DNW, we chose the value of k such that the final learned model has similar Mult-Adds as the base model. For the proposed method, we also set the value of λ in the same manner. Table 2 shows the experimental results on CIFAR-10. We ran each experiments 5 times; the results represent the average and standard deviation. Our approach is denoted DS. DS without the rectified gradient method corresponds to DNW-No Update, where hallucinated edges are not updated. Even without the rectified gradient, the performance of the proposed method is close to that of DNW with the update rule. This finding validates the effectiveness of our sparse parameterization. We also performed experiments with the proximal gradients in Eq.(3) and Eq.(7), which is denoted PG in Table 2. PG- l_1 -norm also uses the l_1 -norm as a regularizer, but the approach did not learn as effectively as ours. Similarly, PG- $l_{1,2}$ -norm uses the update rule of Eq.(7), the shape of which is similar to the proposed sparse parameterization in Eq. (12), but the performance of that method is worse than ours. The results of more experiments, including CIFAR-100, are shown in the supplementary materials due to page limitations.

DNW determines the size and structure of a network by choosing k edges. However, it is not clear how the approach should choose k for different stages (or blocks), so it uses the same pruning rate for all stages. This may be a limitation because each stage plays a different role and may need a different amount of resources. In contrast, our approach controls the model complexity by adjusting the value of λ in the objective function, and a different amount of resources is allocated for each stage through training. As shown in Table 2, the proposed method uses model parameters more efficiently.

4.3 Learning relationship between nodes in a graph convolutional network

In this section, we apply the proposed approach to learn the structure of an adjacency matrix in a graph convolutional network (GCN). The purpose of this case study is to test whether our approach can learn semantic structure from data rather than reducing the size of a neural network or improving the prediction accuracy.



Figure 2: The gray lines represent the 170 road links where the experimental data were collected.

We adopt the model in [11], which is one of the most successful GCN models. A GCN block or layer is defined (see Fig. 1) as

$$H^{l+1} = F(AH^lW^l),$$

where A is an adjacency matrix; H^l and W^l are an input feature and a weight matrix for layer l , respectively; and F is a nonlinear activation function. In general, A is non-negative and shared across GCN blocks. It is obtained by normalization. For example, $A = \tilde{D}^{-1}\tilde{A}$ or $A = \tilde{D}^{-\frac{1}{2}}\tilde{A}\tilde{D}^{-\frac{1}{2}}$, where \tilde{A} is an unnormalized adjacency matrix; and \tilde{D} is a diagonal matrix, where $\tilde{D}_i = \sum_j \tilde{A}_{i,j}$. The adjacency matrix represents the connections or relationships between nodes on a graph and is usually given by prior knowledge. Learning the value of $A_{i,j}$ amounts to determining the relationship between nodes i and j . If the value of $A_{i,j}$ is zero, the two nodes are thought to be unrelated.

As shown in Fig. 1, we define each row and column as a group. Row grouping creates competition between in-coming nodes, whereas column grouping creates competition between out-going nodes. Each row and column of unnormalized adjacency matrix \tilde{A} can be parameterized similarly as in $\tilde{\gamma}$ of in Eq. (10):

$$\begin{aligned} \gamma_{i,j} &= \exp(\alpha_{i,j}) \\ \tilde{A}_{i,j} &= \left(\gamma_{i,j} - \sigma(\beta_i^r) \cdot \|\gamma_{i,:}\|_1 - \sigma(\beta_j^c) \cdot \|\gamma_{:,j}\|_1 \right)_+ \end{aligned}$$

The softmax normalization of Eq. (11) is replaced with Sinkhorn normalization [23, 24, 12] to make A doubly-stochastic (each row and column sum up to 1). After initializing A with \tilde{A} , we can convert \tilde{A} into a doubly stochastic matrix by iteratively applying the following equations:

$$A = D_r^{-1}A \text{ and } A = AD_c^{-1},$$

where D_r and D_c are diagonal matrices; $[D_r]_i = \sum_j A_{i,j}$; $[D_c]_j = \sum_i A_{i,j}$. Note that although the normalization is iterative, it is differentiable. Balanced normalization is also possible by iteratively applying

$$A = D_r^{-\frac{1}{2}}AD_c^{-\frac{1}{2}}.$$

Through numerical experiments, we verified that iteratively applying the above equation also makes \tilde{A} doubly stochastic, but we could not find a theoretical justification for this observation. We leave the mathematical proof as an open question for a future work. As competition groups are created in row- and column-wise approaches, a regularized objective function can be written as

$$\mathcal{L}(D, W, A) + \frac{\lambda}{2} \sum_{i=1}^N \left\{ \mathcal{R}(A_{i,:}) + \mathcal{R}(A_{:,i}) \right\},$$

where $W = \{W^l\}$, N is the size of square matrix A , and $A_{i,:}$ and $A_{:,i}$ denote i th row and column vector of A , respectively. We employ l_p -norm (Eq. (14)) with $p = 0.5$ as a regularizer.

To validate our purposed method, we applied a GCN to estimate future traffic speeds in a road network. The traffic speed data were collected from 170 road segments. Thus, the size of an adjacent matrix is 170×170 . A map of the area from which data were collected is shown in Fig. 2. One-step ahead observation is estimated from eight past observations and an output layer generates 170

estimates, one for each road segment. Prediction loss is measured using the mean relative error (MRE). More detailed specifications of the experimental data and our GCN model can be found in the supplementary material.

Three baseline models were used, where two were provided information on the connections between roads and the other was not. For the first baseline, we set the value of $A_{i,j}$ as a constant such that $A_{i,j} = \frac{1}{n_i}$ if node (or road) i and j were adjacent to each other (n_i is the number of neighbors of node i), and $A_{i,j} = 0$ otherwise. The second baseline used a similar approach, but we set $\tilde{A}_{i,j} = \exp(\alpha_{i,j})$ if node i and j were adjacent to each other to ensure that the strengths of the connections were learned. For the third baseline, no connectivity information was given. However, we set $\tilde{A}_{i,j} = \exp(\alpha_{i,j})$ for all i, j regardless of the actual connections. For the proposed method, we parameterized the adjacency matrix as in the third baseline but applied the sparsification technique with l_p -norm for a regularizer. Balanced normalization was applied to all cases except the first baseline, for which the row sum is 1.

To measure the learned relationship between nodes, we propose the following scoring function:

$$\frac{1}{2N} \sum_{i=1}^N \sum_{j=1}^N \left[(A^r + A^c) \odot M^k \right]_{i,j},$$

where $A^r = D_r^{-1}A$, $A^c = AD_c^{-1}$, \odot denotes the element-wise product, and $[M^k]_{i,j} = 1$ if the geodesic distance between node i and j is less than or equal to k , whereas $[M^k]_{i,j} = 0$ otherwise. The maximum value is 1, and the minimum is 0. For example, the first and second baselines always take the maximum value because their adjacency matrices have exactly the same structure as M^1 . We calculated the scores for $k = 1$ and 2. Note that we used A^r and A^c instead of A because a sparsified matrix is not guaranteed to be doubly stochastic even if the original Sinkhorn normalization method is adopted.

Table 3: Traffic speed prediction with GCN.

(a) Baseline models					(b) Proposed method				
Model	#N.Z.	MAPE(%)	L.R.(×100)		λ	#N.Z.	MAPE(%)	L.R.(×100)	
			$k = 1$	$k = 2$				$k = 1$	$k = 2$
I	878	5.6623	100.00	100.00	0.050	1,220	5.4744	87.06	89.94
II	878	5.5160	100.00	100.00	0.075	1,009	5.4957	88.62	91.39
III	28,900	5.6343	13.76	20.87	0.100	835	5.5336	89.79	92.13

The performance of the baseline models is shown in Table 3a. We ran each experiment five times and selected the median among the five lowest validation errors. For the first and second baselines, the road connectivity information is provided, and the number of non-zero elements of the adjacent matrices is 878. Note that the value of the learned relationship for Baselines I and II is constant, but it is shown for reference. The road connectivity information is not given for the third baseline, and the number of non-zero elements of the adjacent matrix is 28,900(= 170 × 170). The performance of the proposed model is shown in Table 3b. The experiment using Baseline III shows that the GCN found a nonlinear mapping between input and target values simply by reducing the prediction loss without learning the semantic relationships between nodes, but the proposed approach learns the relationships between nodes. We further compared the proposed method with the proximal gradient method. The experimental results are shown in the supplementary material.

5 Scope and Limitations

Our aim is not to achieve state-of-the-art performance but to validate the basic idea and broad applicability of the proposed approach. To the best of our knowledge, this is the first fully [sub]-differentiable sparsification method that zeroes out components, and we hope that our work will provide a foundation for future structure learning and model compression methods. The main limitation of our approach is that a sparsity rate cannot be explicitly specified before training, as is

done in conventional pruning approaches. If a specific sparsity rate is required, it should be obtained by trial-and-error. The rectified gradient can be effective as shown in the neural wiring experiments, but it is not clear what cases it applies to. More theoretical analysis is necessary, which we leave for a future work.

6 Conclusion

In this study, we proposed a fully differentiable sparsification method that can simultaneously learn the sparsified structure and weights of deep neural networks. Our proposed method is versatile in that it can seamlessly be integrated into different types of neural networks and used to address various problems.

Acknowledgments and Disclosure of Funding

This research was supported by the National Research Council of Science & Technology (NST) grant by the Korea government (MSIP) (No. CRC-15-05-ETRI).

References

- [1] Martín Abadi, Ashish Agarwal, Paul Barham, Eugene Brevdo, Zhifeng Chen, Craig Citro, Greg S. Corrado, Andy Davis, Jeffrey Dean, Matthieu Devin, Sanjay Ghemawat, Ian Goodfellow, Andrew Harp, Geoffrey Irving, Michael Isard, Yangqing Jia, Rafal Jozefowicz, Lukasz Kaiser, Manjunath Kudlur, Josh Levenberg, Dandelion Mané, Rajat Monga, Sherry Moore, Derek Murray, Chris Olah, Mike Schuster, Jonathon Shlens, Benoit Steiner, Ilya Sutskever, Kunal Talwar, Paul Tucker, Vincent Vanhoucke, Vijay Vasudevan, Fernanda Viégas, Oriol Vinyals, Pete Warden, Martin Wattenberg, Martin Wicke, Yuan Yu, and Xiaoqiang Zheng. TensorFlow: Large-scale machine learning on heterogeneous systems, 2015. URL <https://www.tensorflow.org/>. Software available from tensorflow.org.
- [2] Karim Ahmed and Lorenzo Torresani. Connectivity learning in multi-branch networks. *CoRR*, abs/1709.09582, 2017. URL <http://arxiv.org/abs/1709.09582>.
- [3] Jose M. Alvarez and Mathieu Salzmann. Learning the number of neurons in deep networks. In *NIPS*, 2016.
- [4] Djork-Arné Clevert, Thomas Unterthiner, and Sepp Hochreiter. Fast and accurate deep network learning by exponential linear units (elus). In *ICLR*, 2016.
- [5] Jonathan Frankle and Michael Carbin. The lottery ticket hypothesis: Finding sparse, trainable neural networks. In *ICLR*, 2019.
- [6] Babak Hassibi, David G. Stork, and Gregory J. Wolff. Optimal brain surgeon and general network pruning. In *ICNN*, 1993.
- [7] Kaiming He, Xiangyu Zhang, Shaoqing Ren, and Jian Sun. Deep residual learning for image recognition. In *CVPR*, 2016.
- [8] Kaiming He, Xiangyu Zhang, Shaoqing Ren, and Jian Sun. Identity mappings in deep residual networks. In *ECCV*, 2016.
- [9] Andrew G. Howard, Menglong Zhu, Bo Chen, Dmitry Kalenichenko, Weijun Wang, Tobias Weyand, Marco Andreetto, and Hartwig Adam. Mobilenets: Efficient convolutional neural networks for mobile vision applications. *CoRR*, abs/1704.04861, 2017. URL <https://arxiv.org/abs/1704.04861>.
- [10] Gao Huang, Zhuang Liu, and Laurens van der Maaten. Densely connected convolutional networks. In *CVPR*, 2017.
- [11] Thomas N. Kipf and Max Welling. Semi-supervised classification with graph convolutional networks. In *ICLR*, 2017.

- [12] P. A. Knight. The sinkhorn-knopp algorithm: convergence and applications. *SIAM Journal on Matrix Analysis and Applications*, 30(1), 2008.
- [13] Alex Krizhevsky. Learning multiple layers of features from tiny images. *Technical Report*, 2009.
- [14] Alex Krizhevsky, Ilya Sutskever, and Geoffrey E. Hinton. Imagenet classification with deep convolutional neural networks. In *NIPS*, 2012.
- [15] Gustav Larsson, Michael Maire, and Gregory Shakhnarovich. Fractalnet: Ultra-deep neural networks without residuals. In *ICLR*, 2017.
- [16] Y. LeCun, B. Boser, J. S. Denker, D. Henderson, R. E. Howard, W. Hubbard, and L. D. Jackel. Backpropagation applied to handwritten zip code recognition. *Neural Computation*, 1(4): 541–551, Dec 1989. ISSN 0899-7667. doi: 10.1162/neco.1989.1.4.541.
- [17] Yann LeCun, John S. Denker, and Sara A. Solla. Optimal brain damage. In *NIPS*, 1989.
- [18] Hanxiao Liu, Karen Simonyan, and Yiming Yang. Darts: Differentiable architecture search. In *ICLR*, 2019.
- [19] Zhuang Liu, Jianguo Li, Zhiqiang Shen, Gao Huang, Shoumeng Yan, and Changshui Zhang. Learning efficient convolutional networks through network slimming. In *ICCV*, 2017.
- [20] Zhuang Liu, Mingjie Sun, Tinghui Zhou, Gao Huang, and Trevor Darrell. Rethinking the value of network pruning. In *ICLR*, 2019.
- [21] Neal Parikh and Stephen Boyd. Proximal algorithms. *Found. Trends Optim.*, 1(3):127–239, January 2014. ISSN 2167-3888. doi: 10.1561/24000000003. URL <http://dx.doi.org/10.1561/24000000003>.
- [22] Karen Simonyan and Andrew Zisserman. Very deep convolutional networks for large-scale image recognition. In *ICLR*, 2015.
- [23] R. Sinkhorn. A relationship between arbitrary positive matrices and doubly stochastic matrices. *The annals of mathematical statistics*, 35(2):876–879, 1964.
- [24] R. Sinkhorn and P. Knopp. Concerning nonnegative matrices and doubly stochastic matrices. *Pacific Journal of Mathematics*, 21(2), 1967.
- [25] Huizi Mao Song Han and William J. Dally. Deep compression: Compressing deep neural network with pruning, trained quantization and huffman coding. In *ICLR*, 2016.
- [26] John Tran Song Han, Jeff Pool and William Dally. Learning both weights and connections for efficient neural network. In *NIPS*, 2015.
- [27] Christian Szegedy, Wei Liu, Yangqing Jia, Pierre Sermanet, Scott Reed, Dragomir Anguelov, Dumitru Erhan, Vincent Vanhoucke, and Andrew Rabinovich. Going deeper with convolutions. In *CVPR*, 2016.
- [28] Robert Tibshirani. Regression shrinkage and selection via the lasso. *Journal of the Royal Statistical Society. Series B (Methodological)*, 58(1):267–288, 1996.
- [29] Wei Wen, Chunpeng Wu, Yandan Wang, Yiran Chen, and Hai Li. Learning structured sparsity in deep neural networks. In *NIPS*, 2016.
- [30] Mitchell Wortsman, Ali Farhadi, and Mohammad Rastegari. Discovering neural wirings. In *NeurIPS*, 2019.
- [31] Xia Xiao, Zigeng Wang, and Sanguthevar Rajasekaran. Autoprune: Automatic network pruning by regularizing auxiliary parameters. In *NeurIPS*, 2019.
- [32] Saining Xie, Ross Girshick, Piotr Dollar, Zhuowen Tu, and Kaiming He. Aggregated residual transformations for deep neural networks. In *CVPR*, 2017.

- [33] Jaehong Yoon and Sung Ju Hwang. Combined group and exclusive sparsity for deep neural networks. In *ICML*, 2017.
- [34] Yang Zhou, Rong Jin, and Steven Chu–Hong Hoi. Exclusive lasso for multi-task feature selection. In *AISTATS*, 2010.

Appendix: Differentiable Sparsification for Deep Neural Networks

Yongjin Lee

Electronics and Telecommunications Research Institute
281 Gajeong-ro, Yuseong-gu, Daejeon, Korea 34129
solarone@etri.re.kr

Abstract

This is the appendix for *Differentiable Sparsification for Deep Neural Networks*.

1 Sparsity Regularizer

In our approach, different sparsity patterns can be derived by adopting different norms for a regularizer. For example, an individual component (e.g., a channel) can be removed by l_1 -norm and a group of components or an entire module (e.g., a layer) can be zeroed-out by $l_{2,1}$ -norm. Note that it is not necessary to manually implement different updating rules as in the proximal gradient approach. Instead, we simply change a regularization term in an objective function. An implementation example with TensorFlow is shown in Listing 1.

```
1 def safe_l2_norm(tensor, axis=None, keepdims=None, name=None):
2     @tf.custom_gradient
3     def norm(x):
4         y = tf.norm(x, 2, axis, keepdims, name)
5
6         def grad(dy):
7             ex_dy = tf.expand_dims(dy, axis) if axis else dy
8             ex_y = tf.expand_dims(y, axis) if axis else y
9             # for numerical stability, add a small constant
10            return ex_dy * (x / (ex_y + 1e-19))
11
12            return y, grad
13
14            return norm(tensor)
15
16 alpha_mag = tf.nn.relu(abs_alpha - sig_beta*alpha_l1)
17 alpha = tf.math.sign(alpha) * alpha_mag
18
19 if norm == 'l1': #l1-norm
20     reg = tf.reduce_sum(alpha_mag)
21 elif norm == 'group': #l2-group norm
22     alpha_mags = tf.reshape(alpha, shape=[len(channels), -1])
23     reg = tf.reduce_sum(safe_l2_norm(alpha_mags, axis=-1))
```

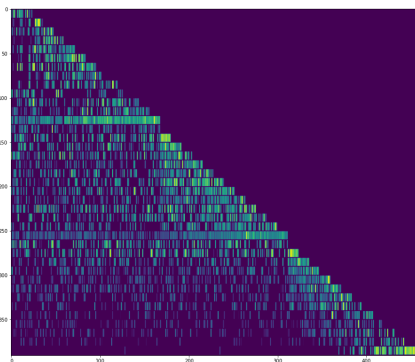
Listing 1: Codes for Regularizer

Figures 1 and 2 show the sparsified structures of DenseNet-K12 with 40 layers, trained with l_1 -norm and $l_{2,1}$ -norm, respectively. Each row corresponds to one hidden layer. For sparse regularization with $l_{2,1}$ -norm, we create a group of 12 channels such that layer-wise connections can be learned. Fig. 1 shows the sparsified structures of the hidden layers in channel-wise. The pixel-like thin short strip represents the magnitude of a scale parameter in the batch normalization. Fig. 2 shows the

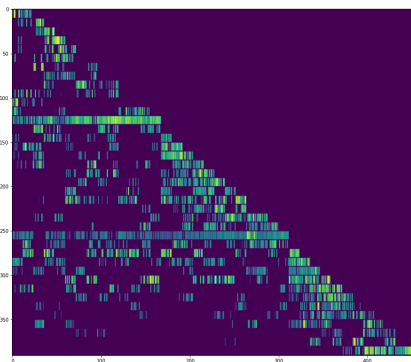
sparsified structures in group-wise. Each square block represents a group of 12 channels. One block is added at a time as a layer proceeds from top to bottom since each layer outputs 12 new channels. An input layer generates 24 channels; thus, the first row has 2 blocks. The number of surviving channels is represented by the color of the block, the brightness of which is proportionate to the number of non-zero channels within a group. Table 1 shows the sparsity rates for a base model, Network-slimming(NS) [7] and the proposed method (DS). Although the two cases of the proposed approach have similar channel-sparsity rates, the learned structures are very different. The experimental results show that the proposed sparse parameterization method is not limited to a particular norm and that it can learn different structures by simply changing norms.

Table 1: Sparsity Rate on CIFAR-10, DenseNet-40-K12.

Model	C. Sparsity(%)		G. Sparsity(%)		Top-1 Error(%)		Parmas	
	Avg.	Std.	Avg.	Std.	Avg.	Std.	Avg.	Std.
Base	00.0	0.0	00.0	0.0	5.92	0.20	1.1×10^6	0.0
NS	60.0	0.4	6.0	0.9	5.71	0.16	4.8×10^5	7.7×10^2
DS- l_1	60.3	0.4	6.4	0.3	5.72	0.16	4.7×10^5	3.5×10^3
DS- $l_{2,1}$	60.6	0.4	56.5	0.5	6.28	0.25	4.7×10^5	5.0×10^3

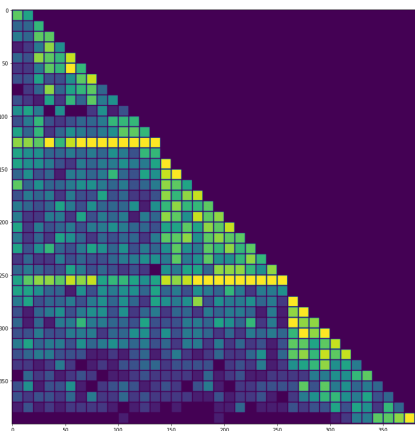


(a) l_1 -norm

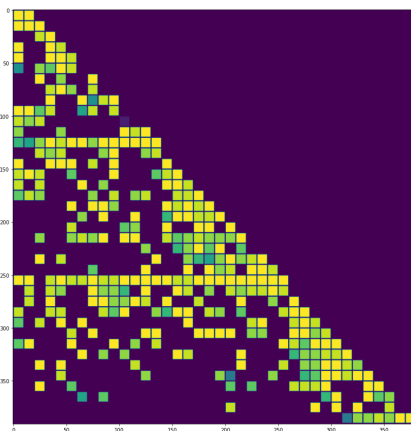


(b) $l_{2,1}$ -group norm

Figure 1: Sparsified connection in channel-wise view. DenseNet-40-K12.



(a) l_1 -norm



(b) $l_{2,1}$ -group norm

Figure 2: Sparsified connection in group-wise view. DenseNet-40-K12.

2 Rectified Gradient Flow

2.1 Implementation

Listing 2 shows the TensorFlow implementation of the rectified gradient flow. The learning method can be implemented by simply switching `tf.nn.relu` to `rgf_relu`.

```

1 @tf.custom_gradient
2 def rgf_relu(x):
3     o1 = tf.nn.relu(x) # forward-pass
4     o2 = tf.keras.activations.elu(x, alpha=0.1) # backward-pass
5
6     def grad(dy): # the gradient of elu is used in backward-pass
7         return tf.gradients(o2, [x], grad_ys=[dy])
8
9     return o1, grad
10
11 #alpha_mag = tf.nn.relu(abs_alpha - sig_beta*alpha_l1)
12 alpha_mag = rgf_relu(abs_alpha - sig_beta*alpha_l1)

```

Listing 2: Rectified Gradient Flow Code

2.2 Analysis of Gradient Flow

Assume that an output y of a neuron in a hidden layer is written as

$$y(\mathbf{x}) = \sum_{i=1}^n a_i f_i(\mathbf{x}; \mathbf{w}_i),$$

where \mathbf{x} denotes an input from a preceding layer, \mathbf{w}_i represents the model parameters for component f_i , and a_i is an edge or an architecture parameter. A loss function can be denoted

$$\mathcal{L}(a(\alpha), f(\mathbf{x}; \mathbf{w})).$$

Let a_i be a function of α ,

$$a_i(\alpha_i) = \text{sign}(\alpha_i) (|\alpha_i| - \sigma(\beta))_+,$$

which is simplified for this analysis. The gradients can be written as

$$\frac{\partial \mathcal{L}}{\partial \alpha_i} = \frac{\partial \mathcal{L}}{\partial y} \cdot \frac{\partial a_i(\alpha_i)}{\partial \alpha_i} \cdot f_i(\mathbf{x}, \mathbf{w}_i), \quad (1)$$

$$\frac{\partial \mathcal{L}}{\partial \mathbf{w}_i} = \frac{\partial \mathcal{L}}{\partial y} \cdot a_i(\alpha_i) \cdot \frac{\partial f_i(\mathbf{x}; \mathbf{w}_i)}{\partial \mathbf{w}_i}, \quad (2)$$

$$\frac{\partial \mathcal{L}}{\partial \mathbf{x}} = \frac{\partial \mathcal{L}}{\partial y} \cdot \sum_j^n \left(a_j(\alpha_j) \cdot \frac{\partial f_j(\mathbf{x}; \mathbf{w}_j)}{\partial \mathbf{x}} \right). \quad (3)$$

If $|\alpha_i| < \sigma(\beta)$, $\partial a_i / \partial \alpha_i$ in Eq. (1) becomes zero and α_i does not have a learning signal. If `elu` [1] is employed in the backward pass, the model can generate an approximate gradient for α_i . Regardless of whether `elu` is used in the backward pass or not, \mathbf{w}_i and \mathbf{x} do not receive a learning signal through a_i since $a_i = 0$ in Eq. (2) and (3). This leads to a similar learning mechanism proposed in DNW [8], where the gradient flows to zeroed-out (hallucinated) edges but not through them.

If we define a as in the main paper,

$$a_i(\alpha) = \text{sign}(\alpha_i) (|\alpha_i| - \sigma(\beta)) \|\alpha\|_1)_+,$$

the gradient is written as

$$\frac{\partial \mathcal{L}}{\partial \alpha_i} = \frac{\partial \mathcal{L}}{\partial y} \cdot \sum_j^n \left(\frac{\partial a_j(\alpha)}{\partial \alpha_i} \cdot f_j(\mathbf{x}, \mathbf{w}_j) \right).$$

Even if `elu` [1] is not used in the backward pass, the gradient for α_i is still generated through others. However, a more effective learning signal can be generated with `elu`.

3 Channel Pruning in a Convolutional Network

We compare the network-slimming (NS) method [7] and our proposed method (DS). We ran each experiment 5 times and show the average and standard deviation. We ensured that DS had similar pruning rate as the NS approach. Tables 2 and 3 show the experimental results on DenseNet with 100 layers [5], and Tables 4 and 5 on ResNet with 164 layers [2, 3]. In the tables, sparsity denotes the pruning rate, i.e, the number of channels that are removed from hidden layers. When the sparsity rate is relatively low, the two approaches have similar error rates, but the difference between them increases as the sparsity rate goes up.

Table 2: Performance on CIFAR-10, DenseNet-100-BC-K12.

Model	Sparsity(%)		Top-1 Error(%)		Parmas		FLOPs	
	Avg.	Std.	Avg.	Std.	Avg.	Std.	Avg.	Std.
Base	00.0	0.0	5.44	0.11	7.6×10^5	0.0	5.8×10^8	0.0
NS	50.0	0.0	5.18	0.14	4.4×10^5	4.6×10^2	3.2×10^8	2.8×10^6
NS	60.0	0.0	5.40	0.14	3.7×10^5	3.3×10^2	2.5×10^8	3.0×10^6
NS	70.0	0.0	6.53	0.19	2.9×10^5	9.3×10^2	1.9×10^8	5.0×10^6
NS	75.0	0.0	7.29	0.27	2.5×10^5	1.0×10^3	1.6×10^8	3.3×10^6
NS	80.0	0.0	8.39	0.28	2.0×10^5	2.0×10^3	1.4×10^8	3.4×10^6
DS	50.2	0.2	5.19	0.13	4.5×10^5	1.3×10^3	3.3×10^8	2.9×10^6
DS	60.4	0.4	5.42	0.20	3.6×10^5	3.5×10^3	2.5×10^8	3.4×10^6
DS	70.3	0.1	5.77	0.09	2.7×10^5	2.3×10^3	1.8×10^8	1.6×10^6
DS	75.7	0.2	6.05	0.26	2.2×10^5	2.6×10^3	1.5×10^8	3.0×10^6
DS	80.4	0.1	6.64	0.11	1.7×10^5	0.6×10^3	1.3×10^8	2.0×10^6

Table 3: Performance on CIFAR-100, DenseNet-100-BC-K12.

Model	Sparsity(%)		Top-1 Error(%)		Parmas		FLOPs	
	Avg.	Std.	Avg.	Std.	Avg.	Std.	Avg.	Std.
Base	00.0	0.0	24.00	0.23	7.9×10^5	0.0	5.8×10^8	0.0
NS	50.0	0.0	23.88	0.19	4.6×10^5	2.7×10^3	2.9×10^8	7.1×10^6
NS	60.0	0.0	25.02	0.26	3.9×10^5	2.0×10^3	2.4×10^8	4.9×10^6
NS	70.0	0.0	28.02	0.75	3.1×10^5	1.5×10^3	1.9×10^8	4.0×10^6
NS	75.0	0.0	29.66	0.51	2.8×10^5	1.1×10^3	1.6×10^8	4.7×10^6
NS	80.0	0.0	31.50	0.46	2.4×10^5	7.9×10^2	1.3×10^8	2.7×10^6
DS	50.1	0.4	24.30	0.17	4.5×10^5	3.5×10^3	3.0×10^8	2.4×10^6
DS	60.5	0.2	24.86	0.20	3.6×10^5	2.9×10^3	2.4×10^8	5.0×10^6
DS	70.4	0.4	26.37	0.15	2.7×10^5	3.5×10^3	1.8×10^8	5.4×10^6
DS	75.3	0.3	27.20	0.06	2.3×10^5	2.9×10^3	1.5×10^8	3.0×10^6
DS	80.3	0.4	28.12	0.23	1.8×10^5	3.5×10^3	1.3×10^8	1.1×10^7

4 Discovering Neural Wiring

Next, we compare Discovering Neural Wiring (DNW) [8] and our proposed method (DS). MobileNetV1 ($\times 0.25$) [4] is employed as a base model and our implementation closely follows that of DNW. In DNW, the value of k was chosen such that the final learned model has similar Mult-Adds as the base model. We also set the value of λ in the same manner. We ran each experiment 5 times and show the average and standard deviation. Tables 6 and 7 show the experimental results.

Table 4: Performance on CIFAR-10, ResNet-164.

Model	Sparsity(%)		Top-1 Error(%)		Parmas		FLOPs	
	Avg.	Std.	Avg.	Std.	Avg.	Std.	Avg.	Std.
Base	00.0	0.0	5.13	0.05	1.7×10^6	0.0	5.0×10^8	0.0
NS	40.0	0.0	5.10	0.13	1.4×10^6	4.8×10^3	3.9×10^8	1.6×10^6
NS	50.0	0.0	5.22	0.11	1.3×10^6	8.6×10^3	3.5×10^8	4.4×10^6
NS	60.0	0.0	5.49	0.06	1.1×10^6	7.9×10^3	2.9×10^8	3.0×10^6
NS	65.0	0.0	5.98	0.23	9.5×10^5	6.0×10^3	2.6×10^8	4.1×10^6
NS	70.0	0.0	6.67	0.19	8.1×10^5	1.4×10^4	2.2×10^8	3.4×10^6
DS	40.2	0.3	4.91	0.03	1.4×10^6	1.1×10^4	3.8×10^8	2.6×10^6
DS	50.4	0.3	4.99	0.08	1.2×10^6	1.0×10^4	3.3×10^8	4.0×10^6
DS	60.7	0.3	5.33	0.15	8.9×10^5	1.7×10^4	2.6×10^8	3.4×10^6
DS	65.4	0.5	5.46	0.11	7.4×10^5	1.3×10^4	2.3×10^8	4.7×10^6
DS	70.5	0.3	5.68	0.21	5.9×10^5	1.8×10^4	1.9×10^8	5.3×10^6

Table 5: Performance on CIFAR-100, ResNet-164.

Model	Sparsity(%)		Top-1 Error(%)		Parmas		FLOPs	
	Avg.	Std.	Avg.	Std.	Avg.	Std.	Avg.	Std.
Base	00.0	0.0	23.23	0.28	1.7×10^6	0.0	5.0×10^8	0.0
NS	40.0	0.0	23.12	0.23	1.5×10^6	1.1×10^3	3.6×10^8	2.4×10^6
NS	50.0	0.0	23.39	0.25	1.4×10^6	4.3×10^3	3.1×10^8	5.2×10^6
NS	60.0	0.0	24.71	0.24	1.2×10^6	5.3×10^3	2.5×10^8	4.8×10^6
NS	65.0	0.0	26.56	0.83	1.2×10^6	4.0×10^3	2.2×10^8	2.3×10^6
NS	70.0	0.0	27.91	0.36	1.1×10^6	3.7×10^3	1.9×10^8	5.7×10^5
DS	40.6	0.2	23.02	0.05	1.5×10^6	2.2×10^3	3.4×10^8	4.1×10^6
DS	50.8	0.3	23.47	0.20	1.3×10^6	1.1×10^4	3.0×10^8	4.2×10^6
DS	59.6	1.0	24.52	0.08	1.0×10^6	3.1×10^4	2.4×10^8	1.1×10^7
DS	66.0	1.0	24.97	0.32	8.0×10^5	2.1×10^4	2.0×10^8	1.0×10^7
DS	70.8	1.5	25.44	0.40	6.3×10^5	1.9×10^4	1.8×10^8	1.3×10^7

5 Learning relationship between Nodes in Graph

5.1 Data

A summary of the data reported in the main paper is shown in Table 8. There were approximately 70,000 probe taxis operating in the metropolitan area where the data were collected. As the taxis operated in three shifts, more than 20,000 probes on average ran at any given point in time. The traffic speed data covers 4,663 links in the area, which includes major arterials. Speed data from probes in the metropolitan area were aggregated every 5 minutes for each road segment; if no probe passed a link during a 5-minute period, the speed was estimated based on speeds in the previous time periods or from the same time periods in the past. After preprocessing, the raw data were once again aggregated in 15-minute periods to maximize forecasting utility. A 15-minute period is the standard on which the highway capacity manual is based. As no information was available regarding probe counts, which contribute to averaging speed data, three speeds for a 5-minute period were averaged without weighting. Among the 4,663 links for which speed data were available, we selected 170 links in the subarea (see Fig. 3). We expected that the speed data collected in this region would be free from missing observations as it is the busiest region in the metropolitan area, and most taxi drivers congregate in this region to find passengers. Following the generic conventions of machine learning, we used data from the previous eight months to train the proposed model and reserved the data for the latter two months to test the trained model.

Table 6: Performance on CIFAR-10, Discovering Neural Wiring

Model	Top-1 Error(%)		Parmas		Mult-Adds	
	Avg.	Std.	Avg.	Std.	Avg.	Std.
MobileNetV1($\times 0.25$)	13.44	0.24	2.2×10^5	0.0	3.3×10^6	0.0
DNW($\times 0.225$)						
No Update Rule	13.86	0.27	2.2×10^5	3.7×10^1	4.5×10^6	3.7×10^4
With Update Rule	10.30	0.20	1.8×10^5	6.7×10^1	3.1×10^6	4.6×10^4
$\lambda \times 10^{-3}$ Proximal Gradient with l_1 -norm						
1.875	11.64	0.41	2.4×10^4	9.0×10^2	3.7×10^6	1.3×10^5
1.950	11.95	0.42	2.3×10^4	1.5×10^3	3.7×10^6	2.6×10^5
2.225	12.17	0.44	2.1×10^4	9.4×10^2	3.3×10^6	1.7×10^5
2.325	12.50	0.28	1.9×10^4	5.7×10^2	3.2×10^6	1.1×10^5
2.400	12.66	0.38	1.8×10^4	1.1×10^3	3.0×10^6	6.4×10^4
$\lambda \times 10^{-3}$ Proximal Gradient with $l_{1,2}$ -norm						
1.250	12.15	1.17	1.0×10^5	1.3×10^4	3.7×10^6	1.2×10^5
1.375	13.14	0.42	9.6×10^4	1.2×10^4	3.6×10^6	2.1×10^5
1.500	13.62	0.56	9.6×10^4	1.6×10^4	3.4×10^6	8.6×10^4
1.625	14.12	0.62	8.7×10^4	8.6×10^3	3.3×10^6	1.6×10^5
1.750	15.09	1.21	8.7×10^4	1.5×10^4	3.2×10^6	2.0×10^5
$\lambda \times 10^{-5}$ DS-No Rectified Gradient						
1.125	10.20	0.08	6.9×10^4	8.9×10^2	3.6×10^6	4.9×10^4
1.375	10.55	0.23	6.1×10^4	5.7×10^2	3.4×10^6	4.5×10^4
1.625	10.96	0.18	5.6×10^4	1.7×10^3	3.2×10^6	5.3×10^4
1.875	11.06	0.45	5.1×10^4	2.4×10^2	3.1×10^6	3.7×10^4
2.000	11.05	0.25	4.9×10^4	8.0×10^2	3.0×10^6	3.4×10^4
$\lambda \times 10^{-5}$ DS-Rectified Gradient						
6.0	9.04	0.10	5.3×10^4	7.0×10^2	3.5×10^6	4.8×10^4
6.5	9.28	0.38	5.0×10^4	9.8×10^2	3.5×10^6	7.8×10^4
7.0	9.36	0.27	4.7×10^4	8.4×10^2	3.3×10^6	6.7×10^4
7.5	9.32	0.19	4.5×10^4	3.2×10^2	3.3×10^6	8.5×10^4
8.0	9.66	0.07	4.2×10^4	9.0×10^2	3.1×10^6	6.0×10^4

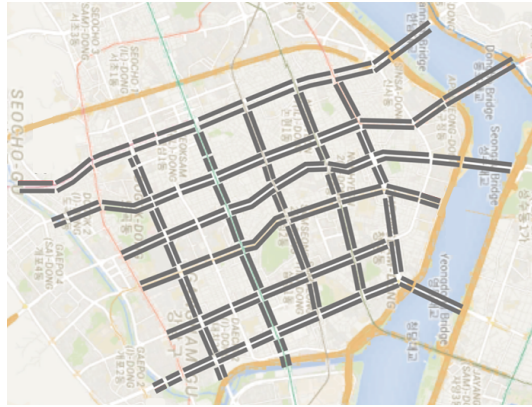


Figure 3: The gray lines represent the 170 road links where the experimental data were collected.

Table 7: Performance on CIFAR-100, Discovering Neural Wiring

Model	Top-1 Error(%)		Parmas		Mult-Adds	
	Avg.	Std.	Avg.	Std.	Avg.	Std.
MobileNetV1($\times 0.25$)	43.78	0.54	2.4×10^5	0.0	3.4×10^6	0.0
DNW($\times 0.225$)						
No Update Rule	40.50	0.30	3.1×10^5	3.8×10^1	4.6×10^6	3.6×10^4
With Update Rule	34.18	0.37	2.6×10^5	5.0×10^2	3.3×10^6	4.7×10^4
$\lambda \times 10^{-3}$			Proximal Gradient with l_1 -norm			
2.1	35.27	0.65	1.3×10^5	4.5×10^3	3.9×10^6	2.6×10^5
2.2	36.00	0.70	1.2×10^5	3.9×10^3	3.6×10^6	9.5×10^4
2.3	35.21	0.32	1.2×10^5	4.1×10^3	3.6×10^6	1.4×10^5
2.4	36.57	0.53	1.2×10^5	4.3×10^3	3.4×10^6	1.9×10^5
2.5	36.81	0.41	1.1×10^5	3.5×10^3	3.2×10^6	2.0×10^5
$\lambda \times 10^{-3}$			Proximal Gradient with $l_{1,2}$ -norm			
1.00	35.97	0.59	3.0×10^5	7.7×10^3	4.4×10^6	1.2×10^5
1.25	37.52	0.84	2.7×10^5	6.3×10^3	3.9×10^6	1.2×10^5
1.50	38.45	0.29	2.6×10^5	5.5×10^3	3.7×10^6	1.1×10^5
1.75	39.63	0.54	2.5×10^5	1.1×10^4	3.5×10^6	1.4×10^5
2.00	41.35	0.86	2.5×10^5	9.7×10^3	3.3×10^6	1.6×10^5
$\lambda \times 10^{-5}$			DS-No Rectified Gradient			
2.00	35.51	0.62	1.8×10^5	5.4×10^2	3.7×10^6	4.8×10^4
2.25	35.26	0.50	1.7×10^5	7.8×10^2	3.5×10^6	4.6×10^4
2.50	35.68	0.47	1.7×10^5	7.5×10^2	3.4×10^6	4.3×10^4
2.75	35.32	0.28	1.6×10^5	5.2×10^2	3.3×10^6	2.5×10^4
3.00	35.77	0.36	1.6×10^5	1.0×10^3	3.2×10^6	2.3×10^4
$\lambda \times 10^{-4}$			DS-Rectified Gradient			
0.850	32.16	0.18	2.0×10^5	3.0×10^3	3.8×10^6	1.2×10^5
0.925	32.84	0.44	1.9×10^5	4.8×10^3	3.6×10^6	8.6×10^4
1.000	32.78	0.83	1.8×10^5	3.3×10^3	3.5×10^6	1.2×10^5
1.125	32.92	0.60	1.6×10^5	4.6×10^3	3.3×10^6	6.8×10^4
1.250	33.80	0.58	1.6×10^5	4.4×10^3	3.1×10^6	8.9×10^4

Table 8: Summary of Experimental Data

Area	# Road Segments	Collection Method	Collection Period	Time Interval	Time Horizon for Prediction
See Fig. 3	170	Taxi with GPS	Jan.-Oct.	15 min.	1 (15 min.)

5.2 Prediction Model with GCN

Figure 4 illustrates our GCN implementation. The outputs of hidden GCN blocks are concatenated and fed to an output block. This was motivated by the dense connections of DenseNet [5]. The structures of the hidden GCN blocks are illustrated in the main paper. We trained the model for 500 epochs using Adam [6] with the defaulting parameter setting of TensorFlow. The initial learning rate was set to 0.0005 and multiplied by 0.5 at epochs 400 and 450.

A training loss is defined by the mean relative error (MRE)

$$\frac{1}{N} \sum_{i=1}^N \frac{|\tilde{y}_i - y_i|}{y_i},$$

where N is the number of road segments and \tilde{y}_i and y_i denote an estimate and actual future observation of travel speed on road segment i , respectively. We ran each experiment five times and selected the median among the five lowest validation errors. We reported the test error from the epoch with the median validation MRE. The report error was re-written in tables with mean absolute percentage error (MAPE) for accessibility purposes; MAPE is defined by multiplying MRE by 100.

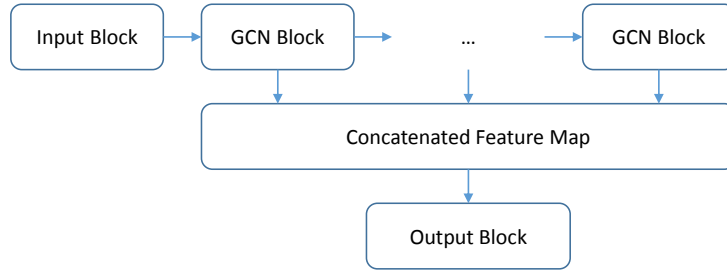


Figure 4: Graph convolutional neural network (GCN) structure. The GCN in our experiments consists of 5 GCN blocks. The output feature maps of GCN blocks are concatenated and then fed to an output block. Input and Output blocks consist of 3 fully connected layers.

5.3 Exclusive Sparsity Regularization

Table 9: Traffic speed prediction with GCN and $l_{1,2}$ -norm regularization

(a) Proximal Gradient					(b) Proposed				
λ	# N.Z.	MAPE(%)	L. R.($\times 100$)		λ	# N.Z.	MAPE(%)	L.R.($\times 100$)	
			$k = 1$	$k = 2$				$k = 1$	$k = 2$
3	12,895	5.3898	57.24	62.42	3	6,170	5.3891	50.75	58.74
5	11,915	5.3933	55.48	60.90	5	5,692	5.3872	52.90	60.86
10	8,723	5.4894	33.39	40.35	10	5,009	5.3999	53.68	61.64
15	7,584	5.5395	13.37	18.05	15	4,704	5.3948	55.83	63.68

The l_p -norm with $p < 1$ can induce strong competition within a group, but its closed-form solution for the proximal operator is unknown. Among the norms which have closed-form solutions, exclusive sparsity regularization can be a promising substitute for l_p -norm with $p < 1$ because of its capacity to promote sparsity or competition within a group. We performed comparative experiments with the $l_{1,2}$ -exclusive norm [10, 9]. As in the main paper, we created groups for the row and column vectors of an adjacency matrix. Note that the proximal operator should be applied to free variables and cannot be applied on γ or a of an adjacency matrix. Thus, we did not apply the exponential function on α and instead constrained the elements of an adjacency matrix to be non-negative by setting the initial values as 1.0 and modifying the proximal operator as

$$\alpha_{g,i} \leftarrow \left(\alpha_{g,i} - \eta \lambda \|\alpha_g\|_1 \right)_+,$$

Table 10: Traffic speed prediction with GCN and $l_{1,2}$ -norm regularization on $\tilde{\gamma}$

λ	# N.Z.	MAPE(%)	L.R.($\times 100$)	
			$k = 1$	$k = 2$
3	1,211	5.4089	70.47	77.04
5	1,161	5.4408	69.73	75.54
10	924	5.4695	70.66	76.24
15	871	5.4696	66.63	72.06

where α_g represents the row or column vector of an adjacency matrix before doubly-stochastic normalization. We applied the proximal operator at every mini-batch after updating the model variables with the gradient of the prediction loss.

As above, we modified our proposed approach for the comparative experiments. We did not employ the exponential function but applied the differentiable thresholding operation described in the main paper,

$$\tilde{\gamma}_{g,i} = \left(\alpha_{g,i} - \sigma(\beta_g) \cdot \|\alpha_g\|_1 \right)_+,$$

where $\tilde{\gamma}_g$ represents the row or column vector of an adjacency matrix before doubly-stochastic normalization. This approach simultaneously optimized the prediction loss and the exclusive sparsity regularizer,

$$\mathcal{R}(\alpha) = \frac{1}{2} \sum_g \|\alpha_g\|_1^2 = \frac{1}{2} \sum_g \left(\sum_i |\alpha_{g,i}| \right)^2.$$

Regularization was applied on α rather than $\tilde{\gamma}$ in order to maintain consistency with the experiment on the proximal operator, where regularization was applied on free variables. Tables 9a and 9b show the experimental results using the proximal gradient and the proposed method, respectively. The proximal method learned the mapping between inputs and targets by reducing the prediction loss, but did not learn the relationship between nodes as well as our method. Our method seeks to strike a balance between the two by directly optimizing the regularized objective, and learns the relationships between nodes more effectively.

Note that it is more appropriate to apply regularization on γ rather than α , as this allows the threshold operator to receive the learning signal directly from the regularization term and better learn how to control the trade-offs. To be certain, we also performed experiments with regularization on $\tilde{\gamma}$ before doubly-stochastic normalization:

$$\mathcal{R}(\tilde{\gamma}) = \frac{1}{2} \sum_g \|\tilde{\gamma}_g\|_1^2 = \frac{1}{2} \sum_g \left(\sum_i |\tilde{\gamma}_{g,i}| \right)^2.$$

The experimental results with exclusive sparsity regularization on $\tilde{\gamma}$ are shown in Table 10. Clearly, direct regularization on $\tilde{\gamma}$ allows the model to better learn the relationships between nodes.

Note that we could not apply $l_{1,2}$ -norm regularization on the row or column vectors of an adjacency matrix after performing doubly-stochastic normalization as the values of $l_{1,2}$ -norm are scaled to 1 by the normalization process. Again, the best approach is to apply regularization on the row or column vectors of an adjacency matrix after doubly-stochastic normalization as in the main paper, but this is not possible for the proximal gradient method, as discussed above. This shows the flexibility of the proposed approach.

References

- [1] Djork-Arné Clevert, Thomas Unterthiner, and Sepp Hochreiter. Fast and accurate deep network learning by exponential linear units (elus). In *ICLR*, 2016.
- [2] Kaiming He, Xiangyu Zhang, Shaoqing Ren, and Jian Sun. Deep residual learning for image recognition. In *CVPR*, 2016.

- [3] Kaiming He, Xiangyu Zhang, Shaoqing Ren, and Jian Sun. Identity mappings in deep residual networks. In *ECCV*, 2016.
- [4] Andrew G. Howard, Menglong Zhu, Bo Chen, Dmitry Kalenichenko, Weijun Wang, Tobias Weyand, Marco Andreetto, and Hartwig Adam. Mobilenets: Efficient convolutional neural networks for mobile vision applications. *CoRR*, abs/1704.04861, 2017. URL <https://arxiv.org/abs/1704.04861>.
- [5] Gao Huang, Zhuang Liu, and Laurens van der Maaten. Densely connected convolutional networks. In *CVPR*, 2017.
- [6] Diederik P. Kingma and Jimmy Lei Ba. Adam: A method for stochastic optimization. In *ICLR*, 2015.
- [7] Zhuang Liu, Mingjie Sun, Tinghui Zhou, Gao Huang, and Trevor Darrell. Rethinking the value of network pruning. In *ICLR*, 2019.
- [8] Mitchell Wortsman, Ali Farhadi, and Mohammad Rastegari. Discovering neural wirings. In *NeurIPS*, 2019.
- [9] Jaehong Yoon and Sung Ju Hwang. Combined group and exclusive sparsity for deep neural networks. In *ICML*, 2017.
- [10] Yang Zhou, Rong Jin, and Steven Chu–Hong Hoi. Exclusive lasso for multi-task feature selection. In *AISTATS*, 2010.